

Elliptic Flow of Identified Hadrons in Au + Au Collisions at $\sqrt{s_{NN}} = 200$ GeV

S. S. Adler,⁵ S. Afanasiev,¹⁷ C. Aidala,⁵ N. N. Ajitanand,⁴³ Y. Akiba,^{20,38} J. Alexander,⁴³ R. Amirkas,¹²
 L. Aphecetche,⁴⁵ S. H. Aronson,⁵ R. Averbeck,⁴⁴ T. C. Awes,³⁵ R. Azmoun,⁴⁴ V. Babintsev,¹⁵ A. Baldisseri,¹⁰
 K. N. Barish,⁶ P. D. Barnes,²⁷ B. Bassalleck,³³ S. Bathe,³⁰ S. Batsouli,⁹ V. Baublis,³⁷ A. Bazilevsky,^{39,15} S. Belikov,^{16,15}
 Y. Berdnikov,⁴⁰ S. Bhagavatula,¹⁶ J. G. Boissevain,²⁷ H. Borel,¹⁰ S. Borenstein,²⁵ M. L. Brooks,²⁷ D. S. Brown,³⁴
 N. Bruner,³³ D. Bucher,³⁰ H. Buesching,³⁰ V. Bumazhnov,¹⁵ G. Bunce,^{5,39} J. M. Burward-Hoy,^{26,44} S. Butsyk,⁴⁴
 X. Camard,⁴⁵ J.-S. Chai,¹⁸ P. Chand,⁴ W. C. Chang,² S. Chernichenko,¹⁵ C. Y. Chi,⁹ J. Chiba,²⁰ M. Chiu,⁹ I. J. Choi,⁵²
 J. Choi,¹⁹ R. K. Choudhury,⁴ T. Chujo,⁵ V. Cianciolo,³⁵ Y. Cobigo,¹⁰ B. A. Cole,⁹ P. Constantin,¹⁶ D. G. d'Enterria,⁴⁵
 G. David,⁵ H. Delagrange,⁴⁵ A. Denisov,¹⁵ A. Deshpande,³⁹ E. J. Desmond,⁵ O. Dietzsch,⁴¹ O. Drapier,²⁵ A. Drees,⁴⁴
 R. du Rietz,²⁹ A. Durum,¹⁵ D. Dutta,⁴ Y. V. Efremenko,³⁵ K. El Chenawi,⁴⁹ A. Enokizono,¹⁴ H. En'yo,^{38,39} S. Esumi,⁴⁸
 L. Ewell,⁵ D. E. Fields,^{33,39} F. Fleuret,²⁵ S. L. Fokin,²³ B. D. Fox,³⁹ Z. Fraenkel,⁵¹ J. E. Frantz,⁹ A. Franz,⁵
 A. D. Frawley,¹² S.-Y. Fung,⁶ S. Garpman,^{29,*} T. K. Ghosh,⁴⁹ A. Glenn,⁴⁶ G. Gogiberidze,⁴⁶ M. Gonin,²⁵ J. Gosset,¹⁰
 Y. Goto,³⁹ R. Granier de Cassagnac,²⁵ N. Grau,¹⁶ S. V. Greene,⁴⁹ M. Grosse Perdekamp,³⁹ W. Guryn,⁵
 H.-Å. Gustafsson,²⁹ T. Hachiya,¹⁴ J. S. Haggerty,⁵ H. Hamagaki,⁸ A. G. Hansen,²⁷ E. P. Hartouni,²⁶ M. Harvey,⁵
 R. Hayano,⁸ X. He,¹³ M. Heffner,²⁶ T. K. Hemmick,⁴⁴ J. M. Heuser,⁴⁴ M. Hibino,⁵⁰ J. C. Hill,¹⁶ W. Holzmann,⁴³
 K. Homma,¹⁴ B. Hong,²² A. Hoover,³⁴ T. Ichihara,^{38,39} V. V. Ikonnikov,²³ K. Imai,^{24,38} L. D. Isenhower,¹ M. Ishihara,³⁸
 M. Issah,⁴³ A. Isupov,¹⁷ B. V. Jacak,⁴⁴ W. Y. Jang,²² Y. Jeong,¹⁹ J. Jia,⁴⁴ O. Jinnouchi,³⁸ B. M. Johnson,⁵ S. C. Johnson,²⁶
 K. S. Joo,³¹ D. Jouan,³⁶ S. Kametani,^{8,50} N. Kamihara,^{47,38} J. H. Kang,⁵² S. S. Kapoor,⁴ K. Katou,⁵⁰ S. Kelly,⁹
 B. Khachaturov,⁵¹ A. Khanzadeev,³⁷ J. Kikuchi,⁵⁰ D. H. Kim,³¹ D. J. Kim,⁵² D. W. Kim,¹⁹ E. Kim,⁴² G.-B. Kim,²⁵
 H. J. Kim,⁵² E. Kistenev,⁴⁸ A. Kiyomichi,⁴⁸ K. Kiyoyama,³² C. Klein-Boesing,³⁰ H. Kobayashi,^{38,39} L. Kochenda,³⁷
 V. Kochetkov,¹⁵ D. Koehler,³³ T. Kohama,¹⁴ M. Kopytine,⁴⁴ D. Kotchetkov,⁶ A. Kozlov,⁵¹ P. J. Kroon,⁵ C. H. Kuberg,^{1,27}
 K. Kurita,³⁹ Y. Kuroki,⁴⁸ M. J. Kweon,²² Y. Kwon,⁵² G. S. Kyle,³⁴ R. Lacey,⁴³ V. Ladygin,¹⁷ J. G. Lajoie,¹⁶
 A. Lebedev,^{16,23} S. Leckey,⁴⁴ D. M. Lee,²⁷ S. Lee,¹⁹ M. J. Leitch,²⁷ X. H. Li,⁶ H. Lim,⁴² A. Litvinenko,¹⁷ M. X. Liu,²⁷
 Y. Liu,³⁶ C. F. Maguire,⁴⁹ Y. I. Makdisi,⁵ A. Malakhov,¹⁷ V. I. Manko,²³ Y. Mao,^{7,38} G. Martinez,⁴⁵ M. D. Marx,⁴⁴
 H. Masui,⁴⁸ F. Matathias,⁴⁴ T. Matsumoto,^{8,50} P. L. McGaughey,²⁷ E. Melnikov,¹⁵ F. Messer,⁴⁴ Y. Miake,⁴⁸ J. Milan,⁴³
 T. E. Miller,⁴⁹ A. Milov,^{44,51} S. Mioduszewski,⁵ R. E. Mischke,²⁷ G. C. Mishra,¹³ J. T. Mitchell,⁵ A. K. Mohanty,⁴
 D. P. Morrison,⁵ J. M. Moss,²⁷ F. Mühlbacher,⁴⁴ D. Mukhopadhyay,⁵¹ M. Muniruzzaman,⁶ J. Murata,^{38,39}
 S. Nagamiya,²⁰ J. L. Nagle,⁹ T. Nakamura,¹⁴ B. K. Nandi,⁶ M. Nara,⁴⁸ J. Newby,⁴⁶ P. Nilsson,²⁹ A. S. Nyanin,²³
 J. Nystrand,²⁹ E. O'Brien,⁵ C. A. Ogilvie,¹⁶ H. Ohnishi,^{5,38} I. D. Ojha,^{49,3} K. Okada,³⁸ M. Ono,⁴⁸ V. Onuchin,¹⁵
 A. Oskarsson,²⁹ I. Otterlund,²⁹ K. Oyama,⁸ K. Ozawa,⁸ D. Pal,⁵¹ A. P. T. Palounek,²⁷ V. S. Pantuev,⁴⁴ V. Papavassiliou,³⁴
 J. Park,⁴² A. Parmar,³³ S. F. Pate,³⁴ T. Peitzmann,³⁰ J.-C. Peng,²⁷ V. Peresedov,¹⁷ C. Pinkenburg,⁵ R. P. Pisani,⁵
 F. Plasil,³⁵ M. L. Purschke,⁵ A. Purwar,⁴⁴ J. Rak,¹⁶ I. Ravinovich,⁵¹ K. F. Read,^{35,46} M. Reuter,⁴⁴ K. Reygers,³⁰
 V. Riabov,^{37,40} Y. Riabov,³⁷ G. Roche,²⁸ A. Romana,²⁵ M. Rosati,¹⁶ P. Rosnet,²⁸ S. S. Ryu,⁵² M. E. Sadler,¹ N. Saito,^{38,39}
 T. Sakaguchi,^{8,50} M. Sakai,³² S. Sakai,⁴⁸ V. Samsonov,³⁷ L. Sanfratello,³³ R. Santo,³⁰ H. D. Sato,^{24,38} S. Sato,^{5,48}
 S. Sawada,²⁰ Y. Schutz,⁴⁵ V. Semenov,¹⁵ R. Seto,⁶ M. R. Shaw,^{1,27} T. K. Shea,⁵ T.-A. Shibata,^{47,38} K. Shigaki,^{14,20}
 T. Shiina,²⁷ C. L. Silva,⁴¹ D. Silvermyr,^{27,29} K. S. Sim,²² C. P. Singh,³ V. Singh,³ M. Sivertz,⁵ A. Soldatov,¹⁵ R. A. Soltz,²⁶
 W. E. Sondheim,²⁷ S. P. Sorensen,⁴⁶ I. V. Sourikova,⁵ F. Staley,¹⁰ P. W. Stankus,³⁵ E. Stenlund,²⁹ M. Stepanov,³⁴ A. Ster,²¹
 S. P. Stoll,⁵ T. Sugitate,¹⁴ J. P. Sullivan,²⁷ E. M. Takagui,⁴¹ A. Taketani,^{38,39} M. Tamai,⁵⁰ K. H. Tanaka,²⁰ Y. Tanaka,³²
 K. Tanida,³⁸ M. J. Tannenbaum,⁵ P. Tarján,¹¹ J. D. Tepe,^{1,27} T. L. Thomas,³³ J. Tojo,^{24,38} H. Torii,^{24,38} R. S. Towell,¹
 I. Tserruya,⁵¹ H. Tsuruoka,⁴⁸ S. K. Tuli,³ H. Tydesjö,²⁹ N. Tyurin,¹⁵ H. W. van Hecke,²⁷ J. Velkovska,^{5,44} M. Velkovsky,⁴⁴
 L. Villatte,⁴⁶ A. A. Vinogradov,²³ M. A. Volkov,²³ E. Vznuzdaev,³⁷ X. R. Wang,¹³ Y. Watanabe,^{38,39} S. N. White,⁵
 F. K. Wohn,¹⁶ C. L. Woody,⁵ W. Xie,⁶ Y. Yang,⁷ A. Yanovich,¹⁵ S. Yokkaichi,^{38,39} G. R. Young,³⁵ I. E. Yushmanov,²³
 W. A. Zajc,^{9,†} C. Zhang,⁹ S. Zhou,^{7,51} and L. Zolin¹⁷

(PHENIX Collaboration)

¹Abilene Christian University, Abilene, Texas 79699, USA

²Institute of Physics, Academia Sinica, Taipei 11529, Taiwan

³Department of Physics, Banaras Hindu University, Varanasi 221005, India

⁴Bhabha Atomic Research Centre, Bombay 400 085, India

- ⁵Brookhaven National Laboratory, Upton, New York 11973-5000, USA
⁶University of California—Riverside, Riverside, California 92521, USA
⁷China Institute of Atomic Energy (CIAE), Beijing, People's Republic of China
⁸Center for Nuclear Study, Graduate School of Science, University of Tokyo, 7-3-1 Hongo, Bunkyo, Tokyo 113-0033, Japan
⁹Columbia University, New York, NY 10027
and Nevis Laboratories, Irvington, New York 10533, USA
¹⁰Dapnia, CEA Saclay, Bâtiment 703, F-91191, Gif-sur-Yvette, France
¹¹Debrecen University, H-4010 Debrecen, Egyetem tér 1, Hungary
¹²Florida State University, Tallahassee, Florida 32306, USA
¹³Georgia State University, Atlanta, Georgia 30303, USA
¹⁴Hiroshima University, Kagamiyama, Higashi-Hiroshima 739-8526, Japan
¹⁵Institute for High Energy Physics (IHEP), Protvino, Russia
¹⁶Iowa State University, Ames, Iowa 50011, USA
¹⁷Joint Institute for Nuclear Research, 141980 Dubna, Moscow Region, Russia
¹⁸KAERI, Cyclotron Application Laboratory, Seoul, South Korea
¹⁹Kangnung National University, Kangnung 210-702, South Korea
²⁰KEK, High Energy Accelerator Research Organization, Tsukuba-shi, Ibaraki-ken 305-0801, Japan
²¹KFKI Research Institute for Particle and Nuclear Physics (RMKI), H-1525 Budapest 114, POBox 49, Hungary
²²Korea University, Seoul, 136-701, Korea
²³Russian Research Center “Kurchatov Institute,” Moscow, Russia
²⁴Kyoto University, Kyoto 606, Japan
²⁵Laboratoire Leprince-Ringuet, Ecole Polytechnique, CNRS-IN2P3, Route de Saclay, F-91128, Palaiseau, France
²⁶Lawrence Livermore National Laboratory, Livermore, California 94550, USA
²⁷Los Alamos National Laboratory, Los Alamos, New Mexico 87545, USA
²⁸LPC, Université Blaise Pascal, CNRS-IN2P3, Clermont-Fd, 63177 Aubiere Cedex, France
²⁹Department of Physics, Lund University, Box 118, SE-221 00 Lund, Sweden
³⁰Institut für Kernphysik, University of Muenster, D-48149 Muenster, Germany
³¹Myongji University, Yongin, Kyonggido 449-728, Korea
³²Nagasaki Institute of Applied Science, Nagasaki-shi, Nagasaki 851-0193, Japan
³³University of New Mexico, Albuquerque, New Mexico 87131, USA
³⁴New Mexico State University, Las Cruces, New Mexico 88003, USA
³⁵Oak Ridge National Laboratory, Oak Ridge, Tennessee 37831, USA
³⁶IPN-Orsay, Université Paris Sud, CNRS-IN2P3, BPI, F-91406, Orsay, France
³⁷PNPI, Petersburg Nuclear Physics Institute, Gatchina, Russia
³⁸RIKEN (The Institute of Physical and Chemical Research), Wako, Saitama 351-0198, Japan
³⁹RIKEN BNL Research Center, Brookhaven National Laboratory, Upton, New York 11973-5000, USA
⁴⁰St. Petersburg State Technical University, St. Petersburg, Russia
⁴¹Universidade de São Paulo, Instituto de Física, Caixa Postal 66318, São Paulo CEP05315-970, Brazil
⁴²System Electronics Laboratory, Seoul National University, Seoul, South Korea
⁴³Chemistry Department, Stony Brook University, SUNY, Stony Brook, New York 11794-3400, USA
⁴⁴Department of Physics and Astronomy, Stony Brook University, SUNY, Stony Brook, New York 11794, USA
⁴⁵SUBATECH (Ecole des Mines de Nantes, CNRS-IN2P3, Université de Nantes) BP 20722 - 44307, Nantes, France
⁴⁶University of Tennessee, Knoxville, Tennessee 37996, USA
⁴⁷Department of Physics, Tokyo Institute of Technology, Tokyo, 152-8551, Japan
⁴⁸Institute of Physics, University of Tsukuba, Tsukuba, Ibaraki 305, Japan
⁴⁹Vanderbilt University, Nashville, Tennessee 37235, USA
⁵⁰Waseda University, Advanced Research Institute for Science and Engineering, 17 Kikui-cho, Shinjuku-ku, Tokyo 162-0044, Japan
⁵¹Weizmann Institute, Rehovot 76100, Israel
⁵²Yonsei University, IPAP, Seoul 120-749, Korea

(Received 16 May 2003; published 30 October 2003)

The anisotropy parameter (v_2), the second harmonic of the azimuthal particle distribution, has been measured with the PHENIX detector in Au + Au collisions at $\sqrt{s_{NN}} = 200$ GeV for identified and inclusive charged particle production at central rapidities ($|\eta| < 0.35$) with respect to the reaction plane defined at high rapidities ($|\eta| = 3-4$). We observe that the v_2 of mesons falls below that of (anti)-baryons for $p_T > 2$ GeV/c, in marked contrast to the predictions of a hydrodynamical model. A quark-coalescence model is also investigated.

DOI: 10.1103/PhysRevLett.91.182301

PACS numbers: 25.75.Dw

Event anisotropy is expected to be sensitive to the early stage of ultrarelativistic nuclear collisions at the BNL Relativistic Heavy Ion Collider (RHIC). The possible for-

mation of a quark-gluon plasma could affect how the initial anisotropy in coordinate space is transferred into momentum space in the final state. The anisotropy parameter

v_2 for a selection of produced particles is derived from the azimuthal distribution of those particles.

$$\frac{dN}{d\phi} \propto 1 + 2v_2 \cos 2(\phi - \Phi_{\text{RP}}), \quad (1)$$

where ϕ is the azimuthal direction of the particle and Φ_{RP} is the direction of the nuclear impact parameter (“reaction plane”) in a given collision. Measurements of the parameter v_2 in RHIC collisions have been performed [1–6] for charged particles and for identified particles. The current work reports results for charged particles versus transverse momentum (p_T) out to 5 GeV/ c , and extends previous measurements for identified particles out to 3 GeV/ c for π and K , and to 4 GeV/ c for protons. (Previous measurements of the v_2 for π , K , and p extended to 1 GeV/ c at $\sqrt{s_{NN}} = 130$ GeV[2].) Detailed measurements of the azimuthal anisotropy are important to eventually discriminate among different possible scenarios for its physical origin. Such scenarios include hydrodynamical flow of compressed hadronic matter, the production of multiple minijets, and an anisotropy developed during an early quark-matter phase of the collision. It has been observed that v_2 saturates at $p_T \sim 2$ GeV/ c and above [4,5]. The cause of this saturation is not yet known; however, we note that at this momentum the particle composition is very different than at low momentum in that the proton yield is comparable to the pion yield [7]. This makes the measurement of v_2 for separately identified particles especially interesting.

The measurements described here were carried out in the PHENIX experiment at RHIC [8]. About 28×10^6 minimum-bias Au + Au collisions at $\sqrt{s_{NN}} = 200$ GeV from the 2001–2002 run period (Run-2) are used in the analysis. Charged particles are measured in the central arm spectrometers ($|\eta| < 0.35$) [9] where PHENIX has excellent particle identification capabilities[10]. The drift chamber and the first pad chamber plane (PC1) together with the collision vertex define the charged particle tracks. In order to reduce background, the reconstructed tracks are confirmed by requiring matching hits in the outer detectors, i.e., the third pad chamber plane (PC3) and the electromagnetic calorimeter or the time-of-flight detector (TOF). In this analysis, the TOF detector is used to identify charged particles up to 4 GeV/ c in p_T . Particle time-of-flight is measured using the TOF with respect to the collision time defined by beam counters (BBC), and is used to calculate mass squared using the particle momentum and the flight path length [7]. The timing resolution of the system is ≈ 120 ps. A momentum dependent $\pm 2\sigma$ cut on mass squared allows particle identification in the following p_T ranges: $0.2 < p_T < 3$ GeV/ c for pions, $0.3 < p_T < 3$ GeV/ c for kaons, and $0.5 < p_T < 4$ GeV/ c for protons. The contamination of misidentified particles is less than 10%. In addition to collision time, the BBC provide z -vertex position infor-

mation. The two beam counters are located at $|z| = 1.5$ m from the collision point, covering $|\eta| = 3-4$. They consist of 64 photomultiplier tubes (PMT) equipped with quartz Cherenkov radiators in front surrounding the beam pipe. The large charged multiplicity (a few hundred) in $|\eta| = 3-4$ and the nonzero signal of event anisotropy in this η range enable us to estimate the azimuthal angle of the reaction plane in each event using the BBC with full azimuthal angle coverage.

Since the v_2 parameter is in effect a quadrupole moment, the anisotropy which gives rise to a nonzero v_2 is often referred to as an “elliptic flow.” It is extracted by first determining the reaction plane angle Φ_{RP} for each event,

$$\tan 2\Phi_{\text{RP}} = \frac{\sum n_{\text{ch}} \sin 2\phi_{\text{PMT}}}{\sum n_{\text{ch}} \cos 2\phi_{\text{PMT}}}, \quad (2)$$

where n_{ch} is the number of charged particles per PMT (determined from the pulse height in each PMT) and ϕ_{PMT} is the azimuthal angle of each PMT. Then, it is calculated by the Fourier moment $v_2 = \langle \cos 2(\phi - \Phi_{\text{RP}}) \rangle$ over all particles, for all events in a given sample [11]. Corrections [11–14] are applied to account for finite resolution in the reaction plane determination, and for possible azimuthal asymmetries in the reaction plane detector response. The bottom-left panel in Fig. 1 shows the average cosine of the difference between the two reaction planes defined by the beam counters at $\eta = 3-4$ and at $\eta = -4-3$ using the elliptic (second) moment definition. In order to improve the reaction plane resolution, a combined reaction plane is defined by averaging the reaction plane angles obtained from each BBC, using the elliptic moment in each. The estimated resolution of the combined reaction plane [11], $\langle \cos 2(\Phi_{\text{meas}} - \Phi_{\text{true}}) \rangle$, has an average of 0.3 over centrality with a maximum of about 0.4. The estimated correction factor, which is the inverse of the resolution

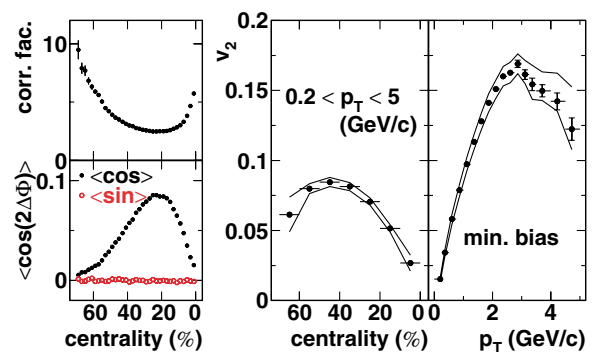


FIG. 1 (color online). Correlation of reaction planes between two beam counters for the second moment is shown as a function of centrality (bottom-left panel) and the correction factor for the combined reaction plane resolution of two beam counters is shown as a function of centrality (top-left panel). The value of v_2 for charged particles is shown as a function of centrality (middle panel) and as a function of p_T (right panel).

for the combined reaction plane, is shown in the top-left panel in Fig. 1.

The present technique is distinguished by defining the reaction plane angle using particles at high rapidity when measuring v_2 for particles at midrapidity. Other measurements of v_2 for midrapidity particles at RHIC have used reaction planes defined with midrapidity particles, or have employed a technique of measuring angular correlations between pairs of particles at midrapidity. While these different approaches generally seek to measure the same thing, they are not identical and a variety of physics effects can cause them to yield different results from the same collision sample [4,15,16]. Because of the large rapidity gap between the reaction plane and the midrapidity acceptance of about three units, it is expected that this analysis is less affected by nonflow contributions. However, we do not observe any substantial difference between the v_2 results shown here and published results for the v_2 of charged particles at RHIC in the p_T range where they are available.

The centrality of each collision is defined using the simultaneous measurement of the total number of particles measured in the BBC and the total energy measured in the zero degree calorimeter [17]. The middle panel in Fig. 1 shows the centrality dependence of v_2 for charged particles measured at midrapidity ($|\eta| < 0.35$) with respect to the reaction plane defined above. The centrality is measured in percentile from the most central collision. The v_2 parameter decreases for both peripheral and central collisions with a maximum at about 50% of the geometric cross section. Beyond 70%, the correction factor due to the reaction plane resolution is large, as shown in the leftmost panel in Fig. 1. This limits the centrality range used in this analysis.

The rightmost panel in Fig. 1 shows the transverse momentum dependence of v_2 for charged particles with respect to the reaction plane for minimum-bias events. The data above a p_T of 2 GeV/c clearly show a deviation from the monotonically increasing behavior seen at smaller p_T . The systematic errors are shown as line bands, which are estimated by several reaction plane methods using the two single beam counters or combined beam counters and by several different ways to correct nonuniform reaction plane distribution: “inverse weighting,” “recentering of sine and cosine summation,” “Fourier expansion,” and combinations of those above [11,18]. Those systematic errors are estimated to be about 10%, depending on centrality, and are independent of p_T . Above 3 GeV/c, background tracks result in an additional systematic error of about 10%, depending on p_T , which is included in the upper error band [19].

In Fig. 2, the transverse momentum dependence of v_2 for identified particles is shown. The top-left panel shows negatively charged particles, while the top-right panel shows positively charged particles as described in the figure caption. The statistical errors and the systematic errors are plotted independently. From the lambda par-

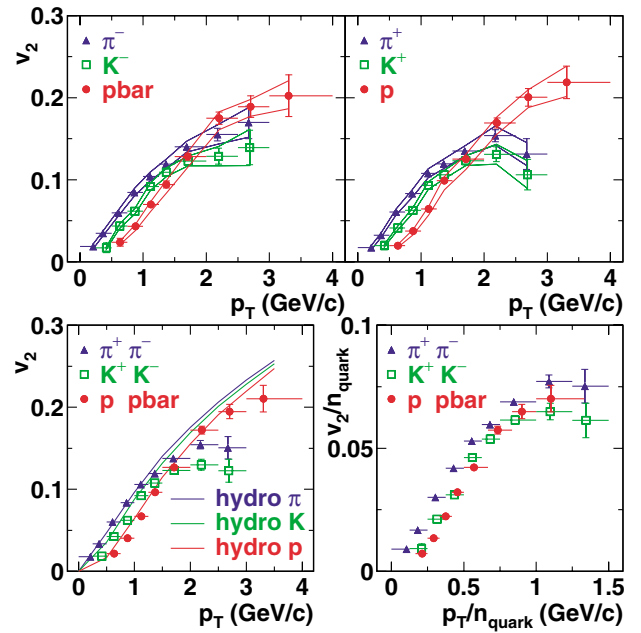


FIG. 2 (color online). Transverse momentum dependence of v_2 for identified particles, π^- , K^- , \bar{p} (top-left panel) and π^+ , K^+ , p (top-right panel). The circles show p and \bar{p} , the squares show K^+ and K^- , and the triangles show π^+ and π^- for minimum-bias events. Statistical errors are represented by error bars and overall systematic error due to all sources by the solid lines in the top two panels. The combined positive particles and negative particles are shown in the bottom-left panel, and the lines there represent the result of a hydrodynamical calculation [20] including a first-order phase transition with a freeze-out temperature of 120 MeV for π , K , and p from upper to lower curves, respectively. The bottom-right panel shows the quark v_2 as a function of the quark p_T by scaling both axes with the number of quarks for each particle, as motivated by a quark-coalescence model [21].

ticle spectra measured in the PHENIX central arm, it is determined that approximately 35% of the protons originate from lambda decays (“lambda feed-down”)[22]. The effect of the lambda feed-down on the measured v_2 of the proton is studied by varying the lambda v_2 with Monte Carlo simulation. Protons resulting from lambda feed-down increase the measured v_2 value. Using the value of the lambda v_2 measured at $\sqrt{s_{NN}} = 130$ GeV at RHIC [3], the effect on the proton v_2 would be less than 10%. Less than 5% of protons originate from decays of particles not involving the lambda. Based on further simulations of their decays to protons, we estimate that the total systematic error due to feed-down is at most 11% depending on p_T , which is included in the lower systematic error band in Fig. 2.

The combined positive and negative particles are shown in the bottom-left panel. The lines in that panel represent a hydrodynamical calculation [20] including a first-order phase transition with a freeze-out temperature of 120 MeV. The data show that at lower p_T (< 2 GeV/c), the lighter mass particles have a larger v_2 at a given p_T ,

which is reproduced by the model calculations. We note, however, that the difference between the charged kaons and charged pions is larger than the model predicts.

A striking feature observed at higher p_T is that the v_2 of p and \bar{p} are larger than for π and K at $p_T > 2$ GeV/ c . This is in sharp contrast to the hydrodynamical picture, which would predict the same mass ordering for v_2 at all p_T . In our data the mesons begin to show a departure from the hydrodynamical prediction at p_T of about 1.5 GeV/ c , while the (anti)baryons agree with the prediction up until 3 GeV/ c but may be deviating at higher p_T . Such behavior is predicted by the quark-coalescence mechanism [21], as shown in the bottom-right panel where both v_2 and p_T have been scaled by the number of quarks. This could be an indication that the v_2 of measured hadrons is already established in a quark-matter phase, although it does not explain why the quark v_2 would saturate with p_T . There exist other scenarios that could be applicable at RHIC, but we have selected two simple models (hydrodynamical and quark coalescence) only to emphasize the experimental evidence of the crossing of v_2 for mesons and baryons.

As an additional illustration of the different behavior for mesons and baryons, the transverse momentum dependences of the v_2 parameter are shown in Fig. 3 for different particles and different centralities. Since the particle identification separation of K and p goes up to 4 GeV/ c , the combined π and K can be compared with protons up to 4 GeV/ c . The charged particle acceptance is larger than the TOF acceptance where the particle

identification can be performed. Therefore, the statistical fluctuations for the charged particle v_2 are smaller than for the p , \bar{p} , and $\pi + K$. The trend exhibited in Fig. 2 for minimum-bias spectra, in which the v_2 for (anti)-baryons exceed those for mesons at $p_T > 2$ GeV/ c , is shown here to occur for all centralities.

In summary, the value of the v_2 parameter for identified and inclusive charged particle production at midrapidity has been measured with respect to the reaction plane defined in the forward and backward rapidity regions in $\sqrt{s_{NN}} = 200$ GeV Au + Au collisions, using the PHENIX experiment at RHIC. The value of v_2 for charged particles decreases for both peripheral and central collisions with a maximum at about the 50th percentile of the geometric cross section. We have observed that for charged particles v_2 increases with p_T up to about 2 GeV/ c , then starts to saturate or decrease slightly. However, the detailed behavior is different for different particle species. The lighter particles have larger v_2 than the heavier particles for p_T below 2 GeV/ c . This trend is partly reversed above 2 GeV/ c where the proton and antiproton have larger v_2 than mesons, a pattern which persists over all centralities. A hydrodynamical calculation can reproduce the mass ordering and magnitude of v_2 for the different particles in the region up to 2 GeV/ c , but fails to reproduce either in the p_T region above 2 GeV/ c . As an alternative, we investigated the quark-coalescence scenario, in which the anisotropy of the final-state hadrons is largely inherited from the anisotropy of quarks in a preceding quark-matter phase. The quark-coalescence model makes a definite prediction for a simple scaling behavior between the v_2 for mesons and for (anti)baryons, and this scaling behavior is largely, though not perfectly, borne out in our data. Further measurements extending to higher p_T involving more identified species will be required to discriminate among alternative scenarios for the origin of elliptic flow at RHIC.

We thank the staff of the Collider-Accelerator and Physics Departments at BNL for their vital contributions. We acknowledge support from the Department of Energy and NSF (U.S.A.), MEXT and JSPS (Japan), CNPq and FAPESP (Brazil), NSFC (China), CNRS-IN2P3 and CEA (France), BMBF, DAAD, and AvH (Germany), OTKA (Hungary), DAE and DST (India), ISF (Israel), KRF and CHEP (Korea), RAS, RMAE, and RMS (Russia), VR and KAW (Sweden), U.S. CRDF for the FSU, US-Hungarian NSF-OTKA-MTA, and US-Israel BSF.

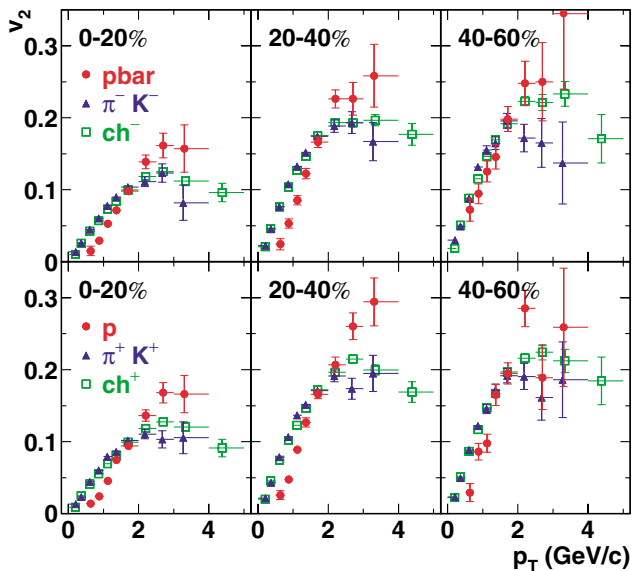


FIG. 3 (color online). Transverse momentum dependence of v_2 for combined π^- and K^- (top) or π^+ and K^+ (bottom) compared with \bar{p} (top) and p (bottom). In addition, results for inclusive negative (top) and positive (bottom) charged particle distributions are plotted as open squares. From left to right, the different centrality selections are shown for 0%–20% (left), 20%–40% (middle), and 40%–60% (right).

*Deceased.

†Spokesperson: zajc@nevis.columbia.edu

- [1] K. H. Ackermann *et al.*, Phys. Rev. Lett. **86**, 402 (2001).
- [2] C. Adler *et al.*, Phys. Rev. Lett. **87**, 182301 (2001).
- [3] C. Adler *et al.*, Phys. Rev. Lett. **89**, 132301 (2002).
- [4] C. Adler *et al.*, Phys. Rev. C **66**, 034904 (2002).

- [5] C. Adler *et al.*, Phys. Rev. Lett. **90**, 032301 (2003).
[6] K. Adcox *et al.*, Phys. Rev. Lett. **89**, 212301 (2002).
[7] K. Adcox *et al.*, Phys. Rev. Lett. **88**, 242301 (2002).
[8] K. Adcox *et al.*, Nucl. Instrum. Methods Phys. Res., Sect. A **499**, 469 (2003).
[9] J.T. Mitchell *et al.*, Nucl. Instrum. Methods Phys. Res., Sect. A **482**, 491 (2002).
[10] H. Hamagaki *et al.*, Nucl. Phys. **A698**, 412 (2002).
[11] A. Poskanzer and S. Voloshin, Phys. Rev. C **58**, 1671 (1998).
[12] J. Barrette *et al.*, Phys. Rev. Lett. **73**, 2532 (1994).
[13] J. Barrette *et al.*, Phys. Rev. C **55**, 1420 (1997).
[14] J. Barrette *et al.*, Phys. Rev. C **56**, 3254 (1997).
[15] N. Borghini, P. M. Dinh, and J. Y. Ollitrault, Phys. Rev. C **63**, 054906 (2001).
[16] N. Borghini, P. M. Dinh, and J. Y. Ollitrault, Phys. Rev. C **64**, 054901 (2001).
[17] K. Adcox *et al.*, Phys. Rev. Lett. **86**, 3500 (2001).
[18] S. Esumi *et al.*, Nucl. Phys. **A715**, 599 (2003).
[19] K. Adcox *et al.*, Phys. Rev. Lett. **88**, 022301 (2002).
[20] P. Huovinen, P. F. Kolb, U. W. Heinz, P. V. Ruuskanen, and S. A. Voloshin, Phys. Lett. B **503**, 58 (2001).
[21] D. Molnar and S. Voloshin, nucl-th/0302014.
[22] K. Adcox *et al.*, Phys. Rev. Lett. **89**, 092302 (2002).